Journal of MATERIALS RESEARCH

Article
DOI:10.1557/s43578-023-00908-y

Development, structural and rheological characterization, and in vitro evaluation of the zinc-doped 45S5 bioactive glass-vaseline ointment for potential wound healing applications

Ali Can Özarslan[1,2], Cem Özel[1,2,a)], Melisa Dilara Okumuş[1], Dilşa Doğan[1], Sevil Yücel[1,2]

[1] Faculty of Chemical and Metallurgical Engineering, Department of Bioengineering, Yildiz Technical University, Istanbul, Turkey
[2] Health Biotechnology Joint Research and Application Center of Excellence, Esenler, 34220 Istanbul, Turkey
[a)] Address all correspondence to this author. e-mail: cemozel@yildiz.edu.tr

Received: 16 November 2022; accepted: 2 January 2023

Bioactive glass (BG) has recently been proposed to be used for wound healing with Vaseline®. To accelerate the wound healing by incorporation of the Zinc (Zn) into BG, undoped and 5 wt% zinc-doped 45S5 BG (16 wt%) were prepared with Vaseline® to create the ointments for wound healing as a VBG and VBG-Zn, respectively. The results showed that desired composition, irregular form, and no porous surface have obtained for BGs. FT-IR spectrum of Zn-doped BG demonstrates increasing Network Connectivity due to Zn incorporation. Ointments exhibited pseudoplastic behaviour and viscoelastic characteristic, indicating that ointments have good topical application. Ointments did not toxic effect towards L929 cells in terms of biocompatibility for topical applications. In vitro wound healing assays revealed that VBG-Zn promotes wound healing thanks to incorporation of the Zn accelerates skin wound closure. All findings point to VBG-Zn ointment having a greater potential for wound healing applications.

Introduction

The skin, the largest organ in the body, has a range of key activities that are crucial to the maintenance of the body's defence against external conditions and is also a quite metabolically active organ. It serves as a barrier against chemical and physical threats, stops the loss of vital body fluids, and supports the regulation of body temperature [1–3]. Damage to the surface of the skin causes it to lose its property of protection and following lead wound formation [4–6]. After wound creation, body begins to reestablish as soon as tissue integrity in an attempt to restore the protection function of the skin [7, 8]. Given the large number of skin and wound issues patients, wound healing is still a critical and ongoing topic in modern medicine [9]. Under normal circumstances, the body activates the wound repair system to restore the integrity of injured tissue, but in some cases, the damaged body parts are unable to function on their own due to incomplete wound healing process [10–12]. In recent years, the different types of biomaterials in different forms have been utilized for wound healing applications in such circumstances [13–15]. These biomaterials can have different production methods and different properties, such as nanofibrous scaffolds, hydrogels, foam and spongy scaffolds and composite biomaterials [16]. Polymer hydrogels with strong adhesive properties can be used in combination with solid nanomaterials as a composite biomaterial for many biomedical applications, including haemostasis, wound healing, or organ repair [17, 18].

In order to promote incomplete healing, it is crucial to choose the right biomaterials [19]. Vaseline® (petroleum jelly), a lubricant, was used topically as a moisture insulator for localized skin and wound issues. Vaseline®, which is often used in the medical and cosmetic industries, can be used to make ointments [20, 21]. Because it is moisturizing, hypoallergenic, and protects dry skin from evaporative losses, Vaseline® is a well-known basic ointment for treating wounds [22]. Vaseline® keeps the wound moist to prevent drying out and the formation of a scab, which inhibits the healing process [23]. Vaseline®-coated gauze has been also applied to a variety of wound healing procedures for many years. Vaseline® has been shown to heal wounds by stopping bacteria from spreading in the skin and wounds from sticking to the gauze [22, 24]. Numerous studies have combined

© The Author(s), under exclusive licence to The Materials Research Society 2023

Vaseline® and other substances in order to improve or accelerate wound healing [20, 25–27].

The bioceramic material known as BioGlass®, also known as Bioactive Glass (BG), was originally developed by Hench in 1969 [28]. Thanks to their great biocompatibility and bioactivity, BGs have been utilized for many years especially hard tissue engineering applications in the fields of dental and orthopaedics to replace and repair bones, teeth, and vertebrae [29–32]. The definition of the term "bioactive" is that in biological environments the bioactive glass can develop hydroxyl-carbonate apatite (HCA) in biological and has the capability to release ions [33]. The first and most well-researched composition is 45S5 Bioglass®, which has a weight-percentage (wt%) composition of 45 SiO_2, 24.5 Na_2O, 24.5 CaO and 6 P_2O_5 [34]. BG was initially examined on hard tissue applications, then it was also studied on soft tissue in order to better understand how 45S5 and soft tissue interaction. [35, 36]. It has recently been suggested for application in soft tissue because of the angiogenic function, haemostatic effect, and bioactivity features determined from numerous research about BGs [33, 37–41]. Because of their ability to release specific ions into liquid media, BGs are gaining popularity in wound treatment applications [33]. Inorganic ions that are physiologically necessary to live, including calcium (Ca), boron (B), silicon (Si), and zinc (Zn), can be released from BGs over a prolonged period time to inhibit microbes, promote collagen synthesis, and/or boost the healing of wounds, according to studies in the last years [42–44].

An intelligent method of creating various types of composites for accelerating the wound healing process is the integration of BG into the polymeric or petroleum-based materials. This combines the benefits of both BG and polymeric or petroleum-based materials [33]. In addition to enhancing functionality of the composite, BGs have also the power to modify the composite's overall rheological characteristics [45–47]. In addition, bioactive glass-containing ointments might be used as topical treatments to treat skin wounds [9, 48–51]. Lin et al. investigated the effect of using three different types of BG-Vaseline ointments on both diabetic and normal skin wounds. Vaseline ointment with a 45S5 BG (18 wt%) composite was widely considered as a pioneer biomaterial for skin regeneration due to its excellent interaction with soft tissue. It happens because BG boosted the proliferation of fibroblasts and growth of granulation tissue that is responsible for wound healing. Additionally, melt-derived glass (45S5) showed the fastest rate of wound healing in the first two days compared to sol–gel glass (SGBG-58S) and sol–gel nanoglass (NBG-58S). However, sol–gel glasses demonstrated faster wound healing after the second day in vivo [29].

Another study for normal and diabetic mice was given samples of 45S5 BG-Vaseline ointment by Mao et al. The 45S5 BG-Vaseline ointments were produced by mixing Vaseline (84 wt%) and 45S5 powder (16 wt%). As a result of study, it has been revealed that the ointment treatment made with 45S5 BG accelerates the proliferation and activity of fibroblasts. The results of this study raised the possibility of using 45S5 BG and Vaseline combination to facilitate the healing of wounds [52].

BGs can be used alone or after being coupled with certain-doped ions in the glass structure for soft tissue engineering and it has been observed the effectiveness of ions addition on wound repair [53–56]. A more functional biomaterial that supports healing and is very compatible with the body may be formed by incorporating various ions into BG. Zinc ion (Zn^{2+}) possesses antibacterial and anti-inflammatory properties and plays critical roles in all stages of wound healing, including angiogenesis, membrane repair, and coagulation [57–60].

Different amounts of ZnO (zinc oxide)-doped BG were prepared by Sergia et al. using the melt-quenched technique. It was found that the structure of the BG was unaffected by the addition of ZnO, and that the rate of BG degradation reduced as the proportion of ZnO amounts increased. Zn-doped BG was investigated for antibacterial effect, and it was observed that BG-containing 3.8 mol% ZnO inhibited the growth of *Staphylococcus epidermidis* gram-positive bacteria and did not show cytotoxic effect [61]. In a study by Aina et al. the effect of zinc-doped 45S5 Bioactive glass on endothelial cells was examined by ion release. This investigation revealed that 5 wt% Zn-doped 45S5 is quite efficient in stimulating the proliferation of endothelial cells when compared to 20 wt% Zn-doped 45S5 and undoped 45S5, but the high Zn ions released by 20 wt% Zn-doped 45S5 drastically reduce cell proliferation. Additionally, the quick pH increase generated by 45S5 dissolution may inhibit cell adherence and spreading. In contrast, the decreased dissolving rate of zinc-containing glasses, which results in a lower pH increase, promotes cell adherence and spreading [62].

It is known that the concentration of Zn-doped in BG affects the ions release rate and hydroxy apatite (HA) formation. In the study by Lusvardi et al. it was observed that ion release and HA formation decreased as the amount of ZnO increased, and even no HA was observed at high ZnO ratio [63]. While it was observed that certain ratios of Zn ions accelerated wound healing, it was observed that the wound healing properties of BGs decreased in case of high ratios of ZnO, and it was stated that the ideal ratio of ZnO was found to be 3.8% in moles (~ 5 wt%) for using wound healing applications.

In this study, we prepared undoped 45S5 bioactive glass-Vaseline and Zn-doped 45S5 bioactive glass-Vaseline ointments. We aimed to investigate effect of Zn addition into bioactive glasses in ointments can promote the wound healing. Ointments and bioactive glass were designed, produced, and characterized in terms of, chemical, morphological, rheological, in vitro biocompatibility, and wound healing properties.

© The Author(s), under exclusive licence to The Materials Research Society 2023

Results and discussion

SEM–EDS analysis

The top-view surface morphology and microstructure of BG and BG-Zn particles were examined by SEM–EDS and are displayed in Fig. 1. BG and BG-Zn in the SEM images appeared to be irregular bulks with a heterogeneous surface as is typical for products of the grinding process and showed a dense surface (no porous surface) with indiscriminate size (< 50 µm) [64–66]. The size of bioactive glass particles was assessed using ImageJ over SEM images, as shown in Fig. 1a and b ($n = 50$ evaluated particles). Average values were found 42.32 µm for BG and 35.78 µm for BG-Zn consequence of measurements. As a result, it has been demonstrated that samples with an average particle size of less than 50 µm are prepared with the desired average particle size. The results of the Laser Scattering Particle Size Distribution Analyzer showed that the average particle size of BG is 47.87 ± 3.86 µm, while the average particle size of BG-Zn is 46.54 ± 3.80 µm, which is consistent with the SEM results. It can be clearly seen that there is no observable change in glass morphology with the introduction of ZnO into 45S5 BG. Thus, it can be said that Zn incorporation did not affect the structure of bioactive glass samples. In addition, Sergi et al. stated that the addition of ZnO did not affect the glass structure (softening temperature, glass transition, etc.) [61]. This confirmed that the sintering conditions used for BG can also be successfully used to sinter BG-Zn particles [67]. The morphological (shape, size and dense structure), compositional, and physiological (bioactivity and ion releasing) characteristics of BG and BG-Zn make these particles promising for various therapeutic applications including wound healing in composite form [68, 69].

Semi-quantitative EDS results in Table 1 displayed that the desired elemental composition which includes Si, Ca, Na, and P elements on the surface of BG and BG-Zn desired elemental composition, while the presence of Zn elements (3.48 wt%) was observed in the surface of BG-Zn. EDS analysis proved the presence of desired elements in a suitable amount into the 45S5 glass and confirm that successful incorporation of Zn^{2+} into the 45S5 glass matrix [70]. The EDS results revealed that the compositions of the BG and BG-Zn matched those designed.

XRF analysis

Table 1 shows a quantitative analysis of the existing compositions (wt%) of BG and BG-Zn using XRF and compares them with the designed compositions. XRF analysis of the BG showed that the particles were composed of Si, Ca, Na and P in oxidic form, while BG-Zn showed that the particles were composed of Si, Ca, Na, P and Zn (5.4 wt%) in oxidic form. The XRF analysis findings showed that the compositions of the synthesized BG and BG-Zn were in good agreement with the desired compositions and EDS results, indicating that their compositions were not changed by fast gelation during the synthesis [32, 70].

FT-IR analysis

The chemical functional groups of BG and BG-Zn were confirmed in Fig. 2 using FT-IR analysis. The FT-IR spectra of

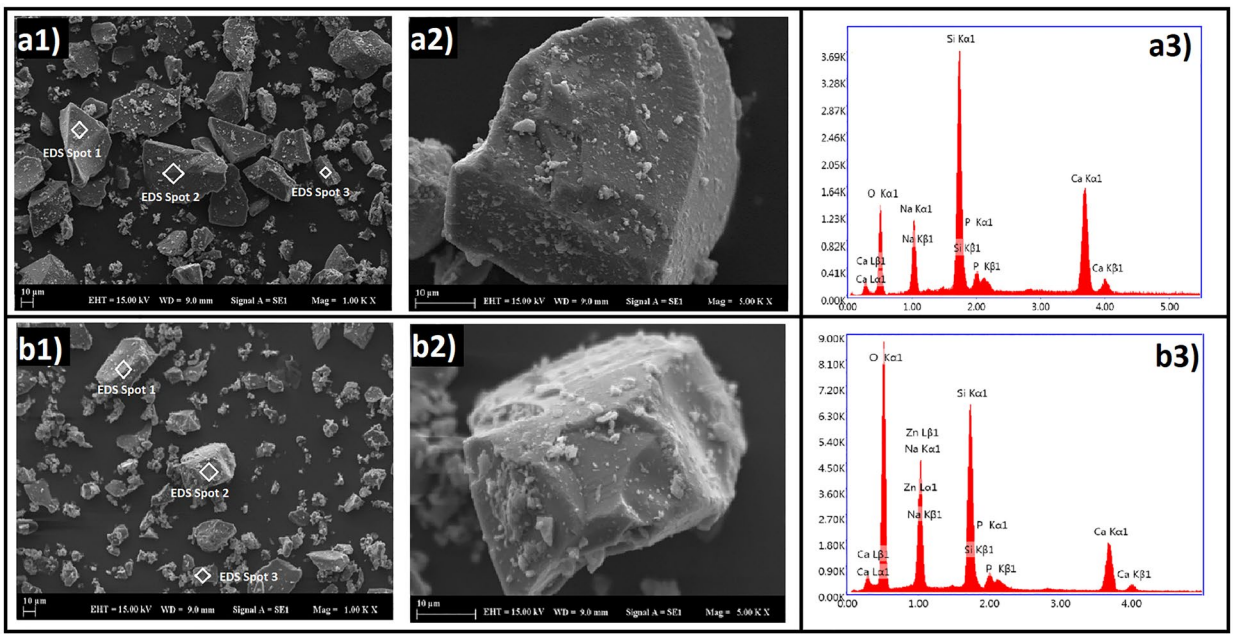


Figure. 1: SEM images of BG and BG-Zn (a1) at × 1000 magnification, (a2) at × 5000 magnification, (b1) at × 1000 magnification, (b2) at × 5000 magnification, respectively. EDS spectrum of BG (a3) and BG-Zn (b3).

© The Author(s), under exclusive licence to The Materials Research Society 2023

TABLE 1: Semi-quantitative analysis of the EDS, quantitative analysis of the composition of bioactive glasses measured by XRF as compared to the designed compositions and network connectivity (NC) value calculated assuming Zn ion to be acting as a modifier and networker by theoretical and experimental.

Theoretical and experimental compositions-determined with EDS and ED-XRF analysis (wt%)						
Samples	BG			BG-Zn		
Composition (wt%)	Design[a]	EDS[b]	XRF[b]	Design	EDS[b]	XRF[b]
SiO_2	45	44.06	44.78	45	44.92	42.30
CaO	24.5	25.46	23.43	22	22.38	21.29
Na_2O	24.5	25.88	24.16	22	22.51	23.37
P_2O_5	6	5.72	5.72	6	4.58	5.51
ZnO	–	–	–	5	3.48	5.40
Calculated network connectivity						
	BG			BG-Zn		
NC'_{theo}	2.12			2.18		
NC'^{*}_{theo}	2.12			2.62		
NC'_{XRF}	2.16			1.99		
NC'^{*}_{XRF}	2.16			2.51		

[a]Indicates designed compositions of BONE-G ACTIVE, REF: BGA025.05/2.

[b]Indicates three replicates.

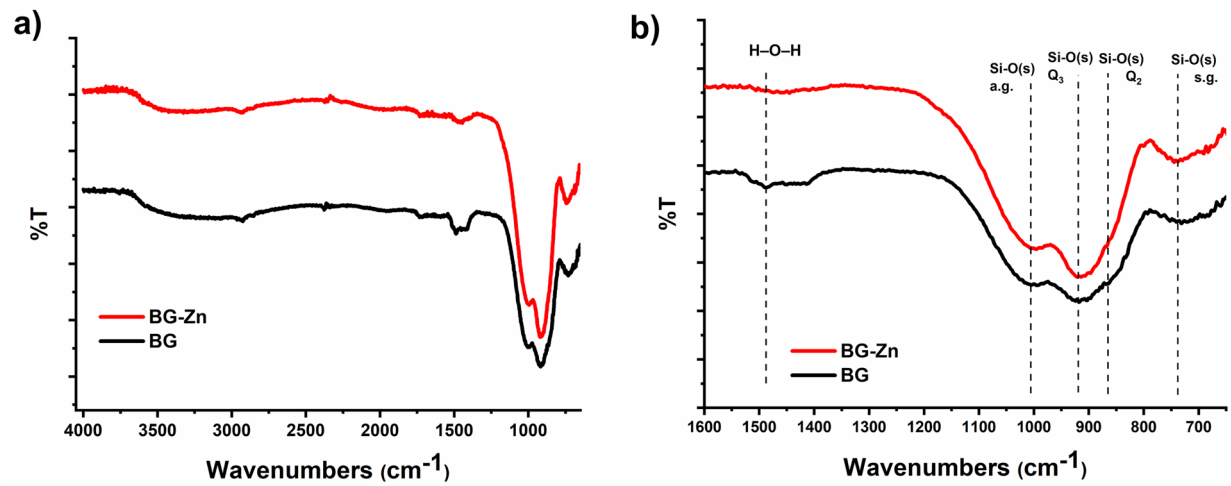


Figure 2: FT-IR spectra of BG and BG-Zn between (a) 4000 and 650 cm^{-1} and (b) 1600 and 650 cm^{-1}.

the BG and BG-Zn showed that main functional groups of 45S5 bioactive glasses have characteristic silicate absorption bands; between 1000 and 1100 cm^{-1}, which corresponds to the asymmetric vibration of the Si–O(s) bond (Si–O a.g.) [71], and between 900 and 950 cm^{-1} the presence of a Si–O(s) bond with one non-bridging oxygen (NBO) per SiO_4 tetrahedron (Q^3) structure and 850 and 870 cm^{-1} the presence of a Si–O(s) bond with two NBO (Q^2) were observed [72]. In addition, Si–O(s)-Q^2 band almost disappeared in BG-Zn spectrum according to BG, which represents decrease in NBO number. This also led to an increase in the NC value, which is expected to cause BG-Zn to dissolve more slowly than BG [73]. Additionally, the deformation vibration of the H–O–H from the water absorbed in the bioactive glass was the source of the band appearing in the region of 1500–1600 cm^{-1} [71, 74]. There has seen no significant change between BG and BG-Zn in the FT-IR spectra [62].

Network connectivity

Glass dissolution and ion release are known to decrease as NC increases due to a less open silicate network, less NBO, and lower concentrations of modifier ions, all of which are essential components of the ion release mechanism seen in bioactive glasses [75]. In the glass structure, ZnO can serve as both a network modifier and networker (an intermediate oxide) [76]. Table 1 shows that the NC values were calculated theoretically and experimentally (with ED-XRF data) of investigated glass samples, and they appear to be in agreement with minor differences (with the exception of NC′ values in the BG-Zn sample).

© The Author(s), under exclusive licence to The Materials Research Society 2023

This difference may be due to the incorporation of Zn in the structure of the produced BG-Zn sample (5.8 wt%) more than the theoretical value (5 wt%). While NC'_{theo} and NC'^{*}_{theo} of BG and BG-Zn were 2.12, 2.12 and 2.18, 2.62, NC'_{XRF} and NC'^{*}_{XRF} values of BG and BG-Zn were 2.16, 2.16 and 1.99, 2.51, respectively. This difference is due to the incorporation of Zn to the glass structure. However, as can be seen, for BG-Zn the NC values varies depending on how Zn is incorporated to the structure. While the NC value increases when Zn act as a co-networker, the NC value increases when Zn serves as a modifier in BG-Zn glass structure. By changing the ZnO content, its function can be converted from that of a modifier to that of networker or vice versa [75]. Studies have shown that by increasing the ZnO content in bioactive glass, the role of Zn changes from a modifier to a networker [70]. When the ZnO level is less than 0.4 mol%, rapid ion release was observed, indicating a rapid in vitro bioactive response [77] while a high Zn content (over 20 wt%) observed that it can significantly reduce the dissolving activity and completely prevent glass from forming HA [62]. Shahrabi et al. have shown that 5 mol% ZnO, which has a similar ratio to our study, can reduce the amount of non-bridging oxygen atoms and, as a result, lower its bioactivity. This was attributed to ZnO are replaced for CaO and it is expected to act as modifier. Therefore, in this structure, Zn ions lead to the formation of tetrahedral ZnO_4^{2-} species that require Ca ions to balance their charges [78]. FT-IR results showed that declining Si–O(s)-Q^2 peak for BG-Zn glass result in increasing experimental NC value. This confirm that Zn is incorporated to the glass structure as modifiers rather than networkers. This indicates that the NC'^{*}_{XRF} value should be considered in NC values. The high NC value of BG-Zn indicates that the bioactivity of bioactive glasses decreases (compared to BG, has slow HCA formation) which might cause from incorporation of Zinc. The studies showed that the increase in the amount of Zn in the bioactive glass decreased the formation of HCA and Hydroxyapatite (HA) structure by affecting the crystallization of the amorphous Ca-P (ACP) layer formed on the surface [62, 79]. In soft tissue application, dissolution of bioactive glasses was welcomed because of that the inorganic ions in the glass are known to have a therapeutic effect on the soft tissue when released, however HCA and HA formation in surface is not always preferable. Furthermore, it is known that HCA formation can inhibit haemostasis in the wound and calcium deposits inhibit the healing of leg ulcers [80–82]. Therefore, for wound healing applications, materials with materials that can dissolve and release therapeutic ions without precipitating HCA will be more effective in wound healing [83]. The high NC value of BG-Zn glass may be associated with low bioactivity due to the slower and/or late degradation of glass [73]. Therefore, BG-Zn glass is expected to have better wound healing properties than BG due to its slow rate of HA formation and therapeutic ion release at the wound site.

Rheological measurements

It is crucial to understand the rheological characteristics of topical applications for wound healing since assessing their viscoelastic parameters, critical stress value, and hysteresis index can be a useful technological tool for predicting their spreading capability on surface of the skin surface [84]. Figure 3 depicts the results of rheological tests performed in rotation mode as shear stress (τ)-shear rate (γ) curves and viscosity (η)-shear rate (γ) curves. The rheological behaviour of VBG and VBG-Zn ointments is similar, as shown in Fig. 3a and b. An increase in shear stress and a decrease in viscosity are observed with shear rate raise for both ointments. This is owing to the fact that Vaseline is a non-Newtonian fluid, a shear-thinning fluid, i.e., a pseudoplastic property [85–88]. VBG-Zn ointment displayed a high viscosity value for the same shear rate, indicating

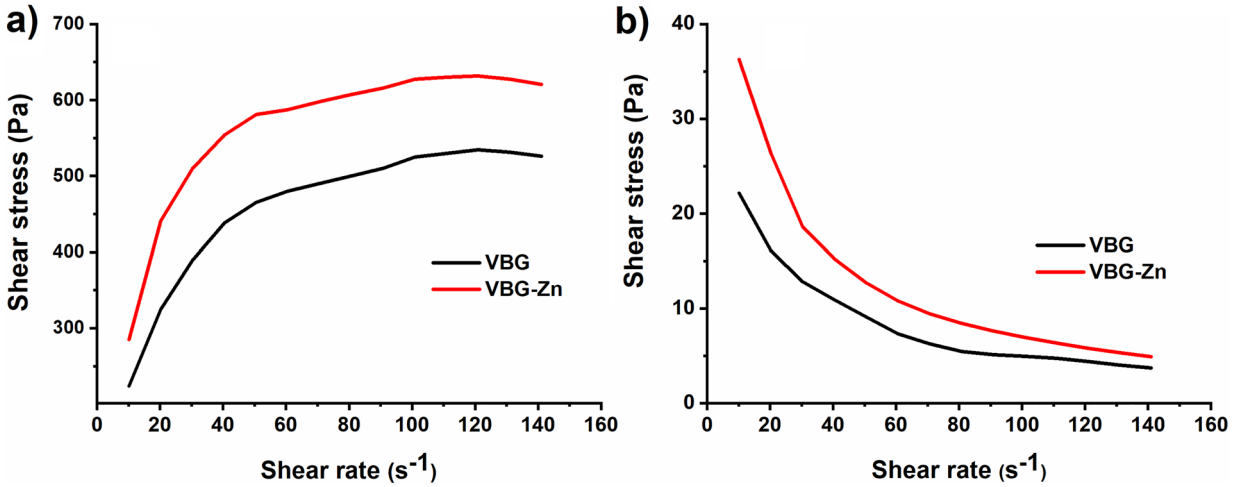


Figure 3: The shear stress-shear rate (a), and the viscosity-shear rate (b) curves of VBG and VBG-Zn samples.

© The Author(s), under exclusive licence to The Materials Research Society 2023

a rather difficult application on the skin surface. Ointment VBG appeared to be more stable than VBG-Zn, suggesting that VBG will quickly regain its original structure following application to the skin. Although VBG demonstrated better fluidity and flow than VBG-Zn, these data imply that both ointments have a good skin application potential [89]. Additionally, fluids with a high bioactive glasses ratio generated a dramatic rise as well as irregular in shear stress with an additional increase in shear rate ($>0.2\ s^{-1}$) [90].

Table 2 lists Ostwald–de Waele equation which contain different parameters including consistency coefficient (k), power-law index (n), and correlation between shear stress-shear rate (R^2) for VBG and VBG-Zn ointments. The data obtained in Table 2 are in good agreement with Fig. 3a and b, therefore, the coefficients of the Ostwald-de Waele equation also support these finding with over 95% correlation rate. According to the equation, viscosity and shear stress increase in direct proportion [91]. The k value, which expresses the resistance of the ointment against flow, increased with the addition of Zn. This is evidence that Zn addition causes significantly increase in the viscosity of the ointments (in Table 2). Furthermore, n values approach to 0 indicating that both ointment samples show non-Newtonian fluid properties (classified as a pseudoplastic) [92]. The results are consistent with previous study. Özarslan et al. discussed that the composition, amount, and particle size of bioactive glasses could affect the fluid features of polymer-ceramic composite systems and stated that addition of melt-quenched bioactive glass in polymers can change fluid type of material [90].

The change in storage (G') and loss (G'') moduli of ointments as a function of angular (or rotational) frequency (ω) are depicted in Fig. 4a and b. For both moduli, it was observed that samples follow a profile that is quite similar. With increasing angular frequency, value of G' and G'' moduli rise. Smaller G' and G'' values were achieved at low oscillation frequencies, and G' increased more rapidly than G''. The G' and G'' moduli were increased dramatically frequency range up to 20 rad/s, but after 20 rad/s G' and G'' moduli was seen a decrease in increasing up to 80 rad/s after which they become almost constant. The granular and irregular shaped form BGs are believed to be responsible for a sudden rise in G' and G'' moduli, which is similar to shear stress. These ointments had viscoelastic behaviour at all angular frequencies, in accordance with the literature reports [93–95], as shown by Fig. 4. Since the storage modulus is consistently greater than the loss modulus at all frequencies ($G' > G''$), the elastic nature of the ointments was found to be superior to their viscous nature [72, 96–99]. However, the amount of increase between G' and G is not very high. Therefore, it can be said that in the range tested, it shows a very weak dependence on the angular frequency [100]. The elastic tendency comes from the Vaseline, while the viscous nature comes from the bioactive glasses. An increase in viscosity has been associated with the addition of bioactive glass, which is typical for colloidal suspensions [101–103]. Briefly, although VBG-Zn and VBG ointments with Zn incorporation showed a viscoelastic structure, Zn incorporation resulted in lower loss and storage moduli.

The complex viscosity (η^*) is the viscosity evaluated as a function of the viscoelastic fluid's oscillation frequency. It displays comprehensive impact of the sample on determining the resistance to shear stress, taking into consideration both the viscous and elastic components of the sample [104, 105]. As can be seen in Fig. 4c, while the complex viscosity of the samples was approximately 4.60 Pa.s at the beginning of the test, it is seen that the complex viscosity decreased with increasing angular frequency in all samples. This is due to the pseudoplastic properties of the ointments [106–109]. These results are consistent with the result of rotation rheology tests.

TABLE 2: The values of k, n and R^2 for ointment samples.

Sample[a]	k (Pa s^n)	n	R^2
VBG	155.72	0.263	0.96
VBG-Zn	297.25	0.184	0.95

[a]Sample analysis were performed three replicates.

In vitro cell viability assay

In vitro cell viability assay was used to determine the cell viability percentage of the ointment samples at different extract concentrations (1.25 mg/ml, 2.5 mg/ml, and 5 mg/ml). The percentage cell viability against extract concentration of results is given in the histogram in Fig. 5. In the MTT experiment, all ointment samples demonstrated high levels of cell mitochondrial activity (>80% of the control), indicating a considerable increase in L929 fibroblast cell viability compared to the control. Thence, both VBG and VBG-Zn samples had non-toxic at certain concentration rates. On the other hand, VBG showed significantly difference ($p<0.05$) according to control on all concentrations. According to significant differences of VBG sample on 1.25, 2.5 and 5 mg/ml concentration, it can be said that the VBG sample was increased cell proliferation related to increasing concentration. Although there was no statistical significance between 1.25 and 2.5 mg/ml concentrations and 2.5 and 5 mg/ml concentrations, there was a statistical significance between 1.25 and 5 mg/ml concentration for VBG-Zn. It might be argued that the VBG-Zn at 5 mg/ml concentration had more cell viability than VBG-Zn at 1.25 mg/ml concentration and in general, increased concentrations of Zn ions, as well as VBG, was shown to improve cell viability when compared to controls.

Wajdo et al. stated that Zn ions (2 and 4 wt%) enhanced the cell viability of Osteoblast-like (MG-63) cells [110]. In our study, VBG-Zn showed higher cell viability than the control

© The Author(s), under exclusive licence to The Materials Research Society 2023

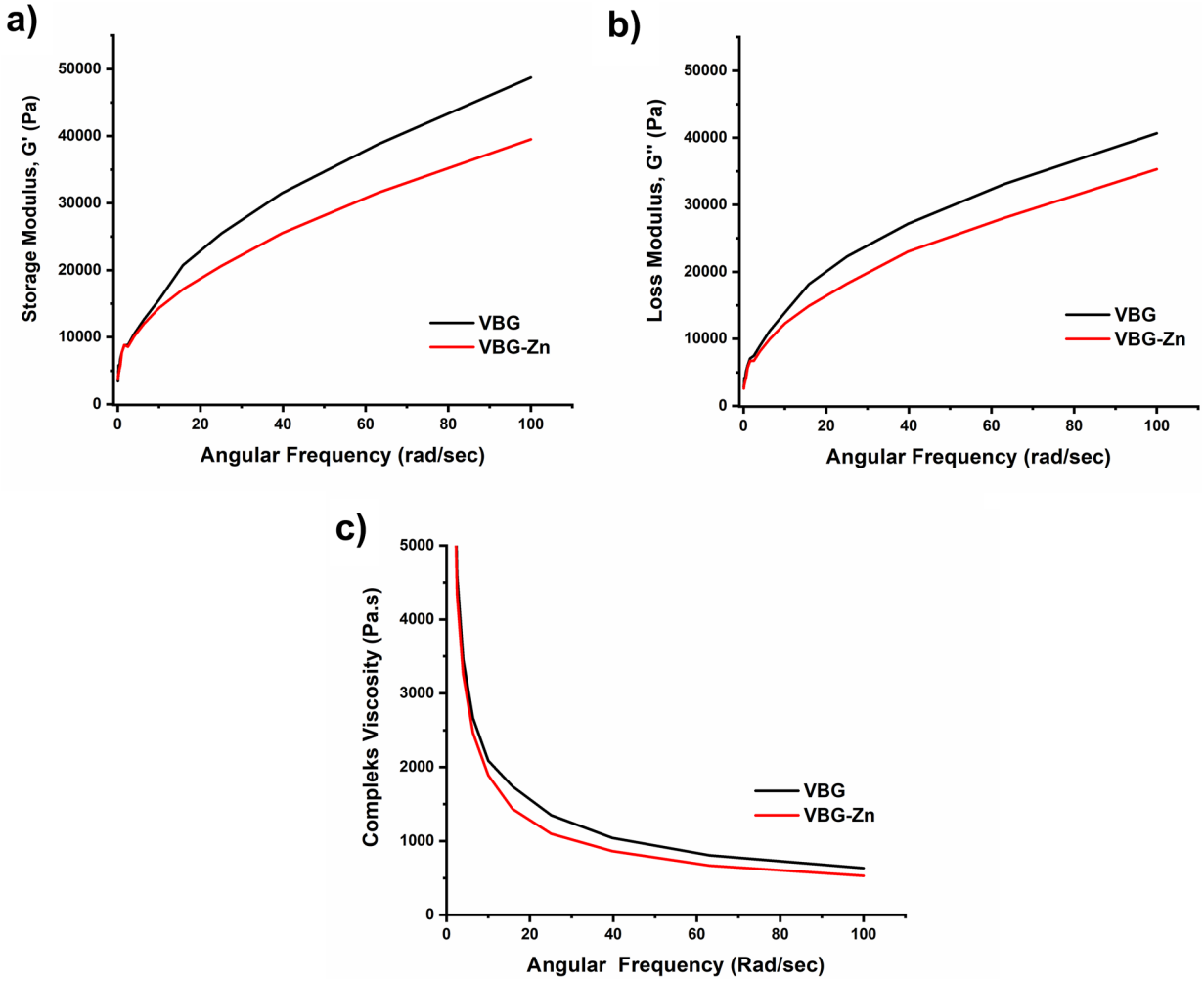


Figure 4: The changes in (a) storage modulus (G′), (b) loss modulus (G″) and (c) complex viscosity (η^*) of VBG and VBG-Zn samples ointments as a function of angular frequency (ω).

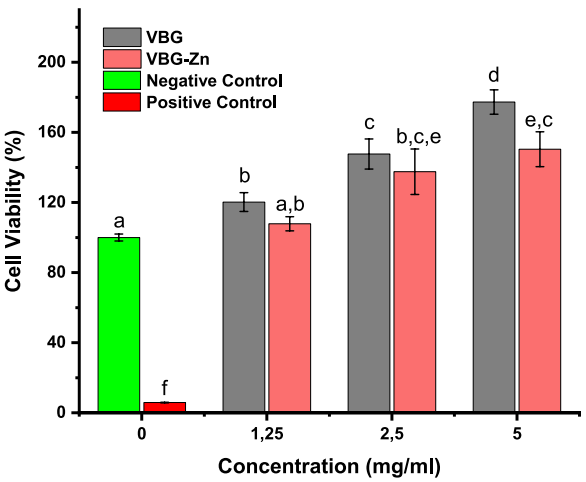


Figure 5: The concentration-dependent cell viability (%) change graph for VBG and VBG-Zn ointment sample after 24 h incubation (data are given as mean ± SD ($n = 3$)—the different letters indicated on the bar represent a statistically significant difference; $p < 0.05$).

while showing lower cell viability than the VBG sample in all concentrations on the L929 cell. The lower cell viability in the absence of Zn can be explained by the fact that Zn is the second most abundant trace metal which is used in lots of metabolic activities while the lower cell viability in the presence of Zn ion can be explicated with leading to cytotoxicity and cell death in excess amount Zn ions [110–112]. Kapoor et al. reported that cell proliferation of the mesenchymal stem cells was adjusted by a dose of Zn ions. They represented that bioactive glass with 4 mol % ZnO was a significantly higher cell viability value with respect to undoped and 8 mol % ZnO bioactive glass [113].

Consequently, it can be said that VBG-Zn in 2.5 and 5 mg/ml concentration and VBG in all concentrations showed an acceleratory effect on the proliferation of cultured L929 cells and it can be understood that the VBG and VBG-Zn Bioactive glass-Vaseline ointment samples can be a biocompatible material due to supporting cell proliferation.

© The Author(s), under exclusive licence to The Materials Research Society 2023

Scratch assay

After demonstrating the non-toxic behaviour of the samples, the effect of VBG and VBG-Zn ointment samples in vitro wound healing activity was evaluated by scratch assay (migration assay) [114, 115]. This assay was performed after 0-, 12-, and 24-h using extracts of VBG and VBG-Zn samples at 5 mg/ml concentrations with observing of migration of the 3T3 mouse fibroblast cells. It is seen that from the optical microscope images in Fig. 6, 3T3 cells showed an increased migration rate with exposure extraction of VBG and VBG-Zn. VBG and VBG-Zn ointment samples at a concentration of 5 mg/ml affect wound closure value (%) depending on time. After 12 h, 33.5% of the fibroblast cells in the control group migrated towards the scratch wound, this number was resulted in 51.5% for VBG and 73.4% for VBG-Zn. Thus, VBG-Zn decreased drastically wound closure time ($^{*}p < 0.05$). While the cells treated with control and VBG had 78.8% and 82% of wound closure after 24 h, almost the entire wound was closed in VBG-Zn ointment treated cells ($^{**}p < 0.05$). Therefore, it is understood that the VBG-Zn ointment sample increased the % wound closure value after both 12- and 24-h incubation more than the VBG ointment sample. Thus, it can be said that Zn doping accelerates the wound healing process in the light of these results. As it is previously described, the introduction of 45S5 bioactive glass (16 wt%) into Vaseline and doping of Zn (5 wt%) into the bioactive glass were seen acceleration of endothelial cells proliferation. Because bioactive glass release Si^{4+} and Na^{+} ions which stimulate angiogenesis and Vascular endothelial growth factor (VEGF) and Zn^{2+} ion could specifically bind to adaptor proteins and stimulate cell migration and adhesion [33, 116]. In addition, as the NC value of BG-Zn shows, the BG-Zn has less bioactivity, therefore it can be said that the release therapeutic ions from VBG-Zn contribute to increased wound healing with slow forming crystalline HA. Because of the aforesaid advantages, the developed system demonstrated by our Zn (5 wt%)-doped 45S5 bioactive glass-Vaseline ointment composite is promising for promoting in vivo wound healing [114].

As a result of these findings, it is understood that BG-containing ointments, regardless of doped or undoped Zn, support and accelerate wound healing rate and VBG-Zn ointment sample also supports faster wound closure by increasing cell migration in 3T3 mouse fibroblast cells compared to VBG ointment sample.

Conclusion

The successful synthesis of BG-Zn with suitable composition was proved by SEM–EDS, FT-IR and XRF analysis and ointments were produced by mixing these glass samples with Vaseline. The VBG and VBG-Zn bioactive glass-Vaseline ointments exhibit pseudoplastic (shear thinning) fluid properties and a viscoelastic structure due to the Vaseline content. Thus, it is thought that the both bioactive glass-Vaseline ointments will provide ease of application to the skin in wound healing application in topical applications due to their pseudoplastic structure. As a result of in vitro cell viability studies, it was observed that both ointments did not show any cytotoxic effect on L929 fibroblast cell line. Accordingly, it is understood that the ointments have biocompatible property indicating safe using in topical applications for wound healing. In addition, scratch analysis experiment on 3T3 mouse fibroblasts performed for

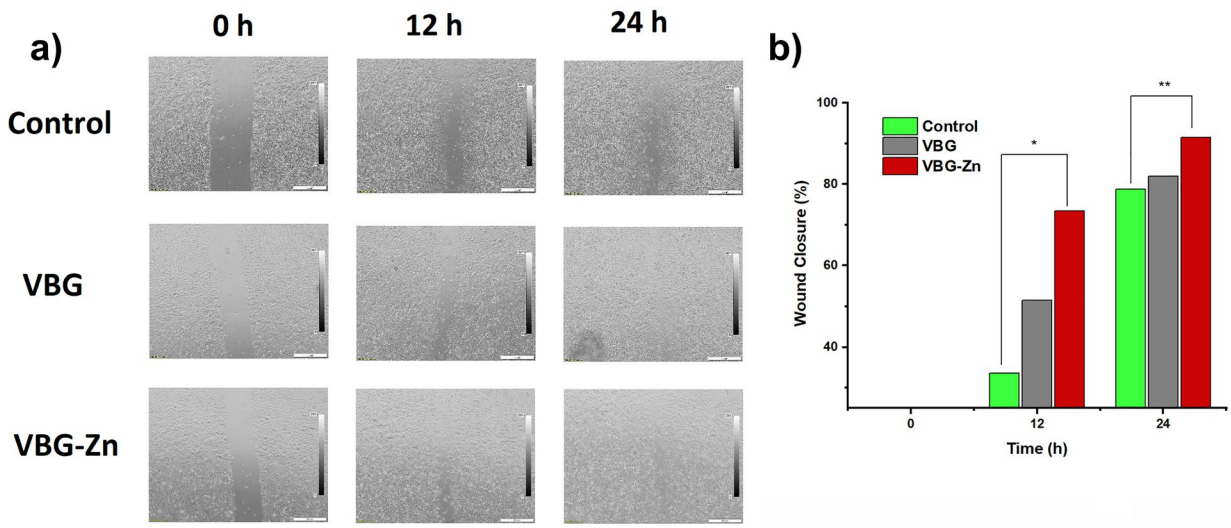


Figure 6: In vitro wound healing activity by scratch assay. (a) Representative microscope images of 3T3 mouse fibroblast cells migration into the scratched area at 0, 12 and 24 h. with treatment VBG and VBG-Zn ointment samples with 5 mg/ml extract concentration. (b) Quantification of wound closure ratio (%) in 3T3 scratch assay (data are given as mean ± SD ($n = 3$), * and **Statistical significance level was determined as $p < 0.05$).

© The Author(s), under exclusive licence to The Materials Research Society 2023

in vitro wound healing activity showed that ointments containing bioactive glass positively affect wound healing. Moreover, it was observed that VBG-Zn was more effective in terms of wound healing rate than VBG, which was thought to be thanks to incorporation of the Zn accelerates skin wound closure. This is due to both the angiogenesis and wound healing properties of Zn ion and the therapeutic ion also releases due to the high NC value, i.e., low bioavailability, of Zn in BG-Zn glass, which does not participate in glass network formation but acts as a modifier. In conclusion, the results have been implied that VBG-Zn ointment can be used as a promising material in soft tissue wound healing and may have an important role in soft tissue engineering applications.

Materials and methods

Materials

Sodium bicarbonate ($NaHCO_3$), calcium carbonate ($CaCO_3$), disodium hydrogen phosphate dihydrate ($Na_2HPO_4.2H_2O$), zinc sulphate heptahydrate ($ZnSO_4{\cdot}7H_2O$) were supplied from Merck. Silicon dioxide (SiO_2) was supplied from Sigma-Aldrich. White German Vaseline® to be used in the production of ointment was purchased from Krauterhof. All chemicals were used as received. Deionized (DI) water obtained from water distillation unit (Gesellschaft für Labortechnik mbH, GFL 2002, Germany). Undoped 45S5 bioactive glass particles (BONE-G ACTIVE, REF: BGA025.05/2, particle size range 0.25–0.5 mm) were supplied from Meta Bioengineering and R&D Services Inc. (Turkey).

Synthesis of melt-quenched bioactive glasses

The Zn-doped bioactive glasses were prepared as described our previous study with some modifications, except annealing step [117]. Briefly, melt-quenched bioactive glasses were prepared by mixing the calculated amounts of the precursors SiO_2, $Na_2HPO_4.2H_2O$, $CaCO_3$, $NaHCO_3$ and $ZnSO_4{\cdot}7H_2O$. The compositions of undoped 45S5 (BG), and zinc-doped 45S5 (BG-Zn) bioactive glasses synthesized via melt-quenched process is given in Table 1. The prepared powdered mixture was placed in a platinum pot with a capacity of approximately 40 ml and heated at 1400 °C in a muffle furnace (Protherm Furnace, PLF 110/6, Turkey) for 1 h. The molten material was cast into cold water. Solid and cold samples was dried at 105 °C, then milled and placed again in platinum pot. After, samples were kept again at 1450 °C for 2 h. Resulting, bioactive glasses were ground in agate mortar for size adjustment and then controlling of size was occurred by sieve. Mean size of bioactive glasses was adjusted to diameters less than 50 µm.

The theoretical and experimental network connectivity calculations of bioactive glasses

The Network connectivity (NC) is a measure of the average number of bridging oxygen atoms on each [SiO_4] tetrahedron which are bridging oxygen atoms join two neighbouring polyhedral [118]. NC can give information about prediction of properties, such as bioactivity, surface reactivity, solubility of glass, chemical, and thermal behaviour [119, 120]. The theoretical NC value of BG and BG-Zn systems were calculated using two different assumptions: (1) assuming Zn act as a typical modifier, NC'_{theo}, and (2) assuming Zn present as partially modifier and partially networker with silicate NC'^{*}_{theo} in Eqs. (1 and 2), respectively [73, 75]. The obtained NC value of bioactive glasses was also achieved with same equations using the values from quantitative Energy Dispersive X-ray Fluorescence (ED-XRF) analysis results (as NC'_{XRF} and NC'^{*}_{XRF}).

$$NC' = \frac{4(SiO_2) + 6(P_2O_5) - 2[(Na_2O) + (CaO) + (ZnO)]}{SiO_2}, \quad (1)$$

$$NC'^{*} = \frac{4[(SiO_2) + (ZnO)] + 6(P_2O_5) - 2[(Na_2O) + (CaO) + (ZnO)]}{[(SiO_2) + (ZnO)]}, \quad (2)$$

where SiO_2, P_2O_5, Na_2O, CaO and ZnO are the concentrations of the components in bioactive glasses in mol%.

Preparation of bioactive glass-vaseline ointments

Vaseline was melted at 65 °C. The bioactive glass-Vaseline ointments were fabricated by mixing bioactive glass powder (16 wt%) and melted Vaseline (84 wt%). The bioactive glasses were progressively dispersed in Vaseline continuously stirring until the ointment reached room temperature [52]. The undoped 45S5 bioactive glass-Vaseline and zinc-doped 45S5 bioactive glass-Vaseline ointments were abbreviated as VBG and VBG-Zn, respectively.

Characterizations

The morphological properties of bioactive glasses were determined by utilizing a scanning electron microscopy (SEM; Carl Zeiss, EVO® Ls 10 T, Germany). The instrument was performed at the accelerating voltage of 15 kV and the images were obtained at different magnification rates. All samples were settled in a sputter coater device (Emitech, Emitech K550X, UK) prior to the SEM analysis and gold was sputtered on their surfaces under vacuum. The bioactive glass sizes were measured by Java's ImageJ® software (Version 1.53t, National Institute of Health, USA, https://imagej.nih.gov/ij/download.html). The semi-quantitative elemental compositions were characterized

© The Author(s), under exclusive licence to The Materials Research Society 2023

utilizing the energy dispersive X-ray spectroscopy (EDS; Carl Zeiss, SmartEDX) by point analysis with three different points. One spectrum is given in Fig. 1. The particle size analysis of bioactive glasses was determined by scattering light intensity analysis using Laser Scattering Particle Size Distribution Analyzer (Horiba Scientific, LA-350, Japan), where the transmittance was 89.2%, circulation speed 7 and manual iteration mode.

Elemental analysis of the bioactive glass particles was carried out using an ED-XRF instrument (PANalytical-Minipal4).

The bioactive glasses were analysed by Fourier Transform Infrared Spectrometer (FT-IR; Shimadzu Corporation, IRPrestige-21, Japan) in attenuated total reflection (ATR) mode to detect chemical structures at room temperature. The spectra were obtained in transmission mode and scans range was adjusted from 4000 to 650 cm^{-1} wavenumber and 15 readings were collected at a resolution of 2 cm^{-1}.

Rheological measurements

The rheological measurements of ointment samples were performed in both rotation and oscillation modes using investigated using rheometer device (MCR302, Anton Paar, Austria) at room temperature. The rotation mode in rheometer was used to determine the rheological characterizations of the material at low strain rates. All experiments were performed in rotation mode with parallel plate–plate with each plate diameter of 25 mm. 1 ml of ointment sample put onto lower plate of the rheometer and the gap size between two plates was adjusted at 1 mm. The rheological tests were carried out in shear rate control mode to determine shear stress (σ) and viscosity (η) as a function of shear rate (γ^n). The shear rate was raised linearly from 0 to 1000 s^{-1} for 180 s. The Ostwald-de Waele power-law equation (Eq. 3) was also used to calculate the relationship between shear stress and shear rate [90, 121],

$$\sigma = k \times \gamma^n, \tag{3}$$

where k shows consistency coefficient in Pa s^n and n shows power-law index. A power-law was fitted to a rising curve to get the values of n and k. The value of n in the Eq. (3) indicates the fluid types and is considered a degree of deviation. For n value there are three situations: the material is referred to as (1) Newtonian fluid if the n value is equal to 1; (2) shear-thinning fluid (pseudoplastic) if the n value is less than 1; and (3) shear-thickening fluid if the n value is greater than (dilatant).

The oscillatory rheology test was used to determine the viscoelastic structure of the VBG and VBG-Zn ointments, which plays a crucial role in the spreading process. Oscillatory measurements in frequency sweep mode were used to evaluate viscoelastic characteristics at constant strain value of 0.01% and varying frequencies (0.1–100 s^{-1}). The strain of 0.01% was chosen to prevent destructive tests and to keep frequency fluctuations steady. The moduli of storage (G') (as the elastic component) and loss (G'') (as the viscous component), as well as complex viscosity (η^*), were determined as a function of angular frequency (ω). Measurements for each sample were carried out in 3 parallels.

In vitro cell viability assay

In vitro cell viability assay of the VBG and VBG-Zn ointments were performed on L929 fibroblast cell line by MTT (3-[4, 5-dimethylthiazol-2-yl]-2, 5 diphenyl tetrazolium bromide) method [122, 123]. L929 cells were incubated in DMEM (Dulbecco's Modified Eagle Medium) for 24 h and 37 °C to achieve a 5 mg/ml final concentration of VBG and VBG-Zn and the elution liquid was sterilized before filtering through a 0.22 m filter. L929 fibroblast cells (1×10^5 cell/ml) were seeded into a 96-well plate and incubated for 24 h. Following the incubation time, cells were treated with different concentrations (0, 1.25, 2.5, and 5 mg/ml) of the VBG and VBG-Zn. After 24 h incubation, the MTT cell viability test was performed on cells using 50 µl of MTT dye for each well at 37 °C with 5% CO_2 for 2 h. Then colorimetric density (absorbance value) was measured at 570 nm (reference wavelength 650 nm) using a Microplate Reader. The positive control was 1% phenol solution, whereas the negative control was DMEM. Results have been calculated assuming the negative control as 100% viable.

In vitro wound healing assay

To assess the wound healing activity of the ointments, the scratch (migration) assay was performed on the 3T3 mouse fibroblast cells [114, 124]. 3T3 mouse fibroblast cells (ATCC® CRL-1658™) were grown in DMEM medium containing 10% FBS for 24 h at 37 °C with 5% CO_2 in 6-well plates (5×10^5 cells/well) and used as a model for evaluating in vitro wound healing activity. Following incubation, a linear vertical wound (a scratch) was gently created in the monolayer using a sterile 200 µl plastic pipette tip, and any cellular debris was eliminated using PBS and incubated at 37 °C, 5% CO_2 for 30 min. Then well were washed with medium and incubated again for 30 min. This procedure takes place to lessen the stress that forms on cells. VBG and VBG-Zn were applied to the cells at a dosage of 5 mg/ml. These cells were monitored using an optical microscope (Olympus CKX41, Olympus, Japan) at initial time zero to measure the wound area immediately after scratching (a_0), and at 12, and 24 h (a_Δ) to detect the areas during the treatment. Serum free medium without treatment was utilized as the reference. The captured images were quantified by Java's ImageJ® by measuring the area of the wound to obtain wound closure percentage with cell free wound surface. The migration of cells toward the wounds was expressed as % wound closure ratio (WC) in Eq. (4) [124]:

© The Author(s), under exclusive licence to The Materials Research Society 2023

$$WC\% = [(a_0 - a_\Delta / a_0)] \times 100. \quad (4)$$

Acknowledgments

This study has been financially supported by Scientific and Technological Research Council of Turkey (TUBITAK) and Meta Bioengineering and R&D Services Inc. (University-Industry Cooperation Student Research Project Support Program with project code 2209-B). Cem ÖZEL also thanks the financial support from the TUBITAK under the BIDEB/2211-A Doctoral Domestic Success Scholarship Program with project number 1649B032000005. The authors would like to acknowledge that this paper is submitted in partial fulfilment of the requirements for PhD degree at Yildiz Technical University.

Author contributions

Not applicable.

Funding

This study has been financially supported by Scientific and Technological Research Council of Turkey (TUBITAK) and Meta Bioengineering and R&D Services Inc. (University-Industry Cooperation Student Research Project Support Program with project code 2209-B). Cem ÖZEL also thanks the financial support from the TUBITAK under the BIDEB/2211-A Doctoral Domestic Success Scholarship Program with project number 1649B032000005.

Data availability

The authors confirm that the data supporting the findings of this study are available within the article. Raw data that support the findings of this study are available from the corresponding author, upon reasonable request.

Code availability

Not applicable.

Declarations

Conflict of interest The authors declare no competing financial interests or personal relationships in this paper.

References

1. J.K. Young, K.M. Baldwin, *Elsevier's integrated histology* (Mosby, Maryland Heights, 2007)
2. P.A.J. Kolarsick, M.A. Kolarsick, C. Goodwin, Anatomy and physiology of the skin. J. Dermatol. Nurses Assoc. **3**(4), 203–213 (2011). https://doi.org/10.1097/JDN.0B013E3182274A98
3. C.M. Chuong, B.J. Nickoloff, P.M. Elias, L.A. Goldsmith, E. Macher, P.A. Maderson, J.P. Sundberg, H. Tagami, P.M. Plonka, K. Thestrup-Pedersen et al., What is the 'true' function of skin? Exp. Dermatol. **11**(2), 159–160 (2002). https://doi.org/10.1034/J.1600-0625.2002.00112.X
4. M. Takeo, W. Lee, M. Ito, Wound healing and skin regeneration. Cold Spring Harb. Perspect. Med. **5**(1), a023267 (2015). https://doi.org/10.1101/CSHPERSPECT.A023267
5. S. Guo, L.A. DiPietro, Factors affecting wound healing. J. Dent. Res. **89**(3), 219 (2010). https://doi.org/10.1177/0022034509359125
6. H. Sorg, D.J. Tilkorn, S. Hager, J. Hauser, U. Mirastschijski, Skin wound healing: an update on the current knowledge and concepts. Eur. Surg. Res. **58**(1–2), 81–94 (2017). https://doi.org/10.1159/000454919
7. R.A.F. Clark, K. Ghosh, M.G. Tonnesen, Tissue engineering for cutaneous wounds. J. Investig. Dermatol. **127**(5), 1018–1029 (2007). https://doi.org/10.1038/SJ.JID.5700715
8. C. Theoret, J. Schumacher, Physiology of wound healing, in *Equine Wound Management*, 3rd edn., ed. by C. Theoret, J. Schumacher (Wiley, Hoboken, 2016), pp.1–13. https://doi.org/10.1002/9781118999219.CH1
9. S.M. Mârza, K. Magyari, S. Bogdan, M. Moldovan, C. Peștean, A. Nagy, F. Tăbăran, E. Licarete, S. Suarasan, A. Dreanca et al., Skin wound regeneration with bioactive glass-gold nanoparticles ointment. Biomed. Mater. **14**(2), 025011 (2019). https://doi.org/10.1088/1748-605X/AAFD7D
10. W.J. Ennis, D. Hill, Wound healing: a comprehensive wound assessment and treatment approach. Skin Tissue Eng. Regener. Med. (2016). https://doi.org/10.1016/B978-0-12-801654-1.00012-7
11. N.X. Landén, D. Li, M. Ståhle, Transition from inflammation to proliferation: a critical step during wound healing. Cell. Mol. Life Sci. **73**(20), 3861 (2016). https://doi.org/10.1007/S00018-016-2268-0
12. S. Kadam, K.S. Kaushik, From ouch to ah-ha! understanding wounds, healing, and infections. Front. Young Minds (2020). https://doi.org/10.3389/FRYM.2019.00157
13. P. Kesharwani, A. Bisht, A. Alexander, V. Dave, S. Sharma, Biomedical applications of hydrogels in drug delivery system: an update. J. Drug Deliv. Sci. Technol. **66**, 102914 (2021). https://doi.org/10.1016/J.JDDST.2021.102914
14. L. Liu, C. Wang, Y. Li, L. Qiu, S. Zhou, P. Cui, P. Jiang, X. Ni, R. Liu, X. Du et al., Manganese dioxide nanozyme for reactive oxygen therapy of bacterial infection and wound healing. Biomater. Sci. **9**(17), 5965–5976 (2021). https://doi.org/10.1039/D1BM00683E
15. X. Fang, Y. Liu, M. Zhang, S. Zhou, P. Cui, H. Hu, P. Jiang, C. Wang, L. Qiu, J. Wang, Glucose oxidase loaded thermosensitive hydrogel as an antibacterial wound dressing. J. Drug

© The Author(s), under exclusive licence to The Materials Research Society 2023

Deliv. Sci. Technol. **76**, 103791 (2022). https://doi.org/10.1016/J.JDDST.2022.103791

16. A.O. Ijaola, D.O. Akamo, F. Damiri, C.J. Akisin, E.A. Bamidele, E.G. Ajiboye, M. Berrada, V.O. Onyenokwe, S.Y. Yang, E. Asmatulu, Polymeric biomaterials for wound healing applications: a comprehensive review. J. Biomater. Sci. Polym. Ed. **33**(15), 1998–2050 (2022). https://doi.org/10.1080/09205063.2022.2088528
17. J.H. Kim, H. Kim, Y. Choi, D.S. Lee, J. Kim, G.R. Yi, Colloidal mesoporous silica nanoparticles as strong adhesives for hydrogels and biological tissues. ACS Appl. Mater. Interfaces **9**(37), 31469–31477 (2017). https://doi.org/10.1021/ACSAMI.7B09083/SUPPL_FILE/AM7B09083_SI_001.PDF
18. S. Rose, A. Prevoteau, P. Elzière, D. Hourdet, A. Marcellan, L. Leibler, Nanoparticle solutions as adhesives for gels and biological tissues. Nature **505**(7483), 382–385 (2013). https://doi.org/10.1038/nature12806
19. A. Morales-Burgos, M.P. Loosemore, L.H. Goldberg, Postoperative wound care after dermatologic procedures: a comparison of 2 commonly used petrolatum-based ointments. J. Drugs Dermatol. **12**(2), 163–164 (2013)
20. Q.Q. Fang, X.F. Wang, W.Y. Zhao, B.H. Shi, D. Lou, C.Y. Chen, M.X. Zhang, X. Wang, L. Ma, W.Q. Tan, Development of a chitosan-vaseline gauze dressing with wound-healing properties in murine models. Am. J. Trop. Med. Hyg. **102**(2), 468 (2020). https://doi.org/10.4269/AJTMH.19-0387
21. S.R. Kuppam, The skinny on moisturizers: a brief report. Dermatol. Open J. **5**(1), 1–5 (2020). https://doi.org/10.17140/DRMTOJ-5-138
22. A. Boudjelal, E. Napoli, A. Benkhaled, L. Benazi, R. Bey, D. Gentile, G. Ruberto, In vivo wound healing effect of Italian and Algerian *Pistacia vera* L. resins. Fitoterapia **159**, 105197 (2022). https://doi.org/10.1016/J.FITOTE.2022.105197
23. American Academy of Dermatology Association, in Proper wound care: How to minimize a scar. https://www.aad.org/public/everyday-care/injured-skin/burns/wound-care-minimize-scars. Accessed 17 Oct 2022.
24. C.S. Pak, D.H. Park, T.S. Oh, W.J. Lee, Y.J. Jun, K.A. Lee, K.S. Oh, K.H. Kwak, J.W. Rhie, Comparison of the efficacy and safety of povidone-iodine foam dressing (Betafoam), hydrocellular foam dressing (Allevyn), and petrolatum gauze for split-thickness skin graft donor site dressing. Int. Wound J. **16**(2), 379–386 (2019). https://doi.org/10.1111/IWJ.13043
25. X.F. Wang, M.L. Li, Q.Q. Fang, W.Y. Zhao, D. Lou, Y.Y. Hu, J. Chen, X.Z. Wang, W.Q. Tan, Flexible electrical stimulation device with Chitosan-Vaseline® dressing accelerates wound healing in diabetes. Bioact. Mater. **6**(1), 230–243 (2021). https://doi.org/10.1016/J.BIOACTMAT.2020.08.003
26. S.H. Huang, C.H. Lin, K.P. Chang, S.H. Wu, S.D. Lin, C.S. Lai, S.F. Ou, S.S. Lee, Clinical evaluation comparing the efficacy of Aquacel Ag with Vaseline gauze versus 1% silver sulfadiazine cream in toxic epidermal necrolysis. Adv. Skin Wound Care **27**(5), 210–215 (2014). https://doi.org/10.1097/01.ASW.0000445919.06416.32
27. S.H. Huang, P.S. Yang, S.H. Wu, K.P. Chang, T.M. Lin, S.D. Lin, C.S. Lai, S.S. Lee, Aquacel® Ag with Vaseline gauze in the management of toxic epidermal necrolysis (TEN). Burns **36**(1), 121–126 (2010). https://doi.org/10.1016/J.BURNS.2009.02.018
28. L.L. Hench, The story of bioglass. J. Mater. Sci. Mater. Med. **17**(11), 967–978 (2006). https://doi.org/10.1007/S10856-006-0432-Z
29. C. Lin, C. Mao, J. Zhang, Y. Li, X. Chen, Healing effect of bioactive glass ointment on full-thickness skin wounds. Biomed. Mater. **7**(4), 045017 (2012). https://doi.org/10.1088/1748-6041/7/4/045017
30. E. Güney, C. Emir, D. Altan, S. Yücel, Development of biocomposite tissue scaffolds of collagen/gelatin/boron-doped bioactive glass prepared through solvent casting/particulate leaching method for bone tissue engineering. J. Indian Chem. Soc. **97**(10(c)), 2006 (2020)
31. B. Karakuzu-İkizler, P. Terzioğlu, B.S. Oduncu-Tekerek, S. Yücel, Effect of selenium incorporation on the structure and in vitro bioactivity of 45S5 bioglass. J. Aust. Ceram. Soc. **56**(2), 697–709 (2020). https://doi.org/10.1007/S41779-019-00388-6/FIGURES/8
32. Y. Basaran Elalmis, B. Karakuzu Ikizler, S. Kilic Depren, S. Yucel, I. Aydin, Investigation of alumina doped 45S5 glass as a bioactive filler for experimental dental composites. Int. J. Appl. Glass. Sci. **12**(3), 313–327 (2021). https://doi.org/10.1111/IJAG.16043
33. T. Mehrabi, A.S. Mesgar, Z. Mohammadi, Bioactive glasses: a promising therapeutic ion release strategy for enhancing wound healing. ACS Biomater. Sci. Eng. **6**(10), 5399–5430 (2020). https://doi.org/10.1021/ACSBIOMATERIALS.0C00528/ASSET/IMAGES/LARGE/AB0C00528_0008.JPEG
34. L.L. Hench, J.M. Polak, Third-generation biomedical materials. Science **295**(5557), 2002 (1979). https://doi.org/10.1126/SCIENCE.1067404
35. L.L. Hench, L.L. Hench, Chronology of bioactive glass development and clinical applications. New J. Glass Ceram. **3**(2), 67–73 (2013). https://doi.org/10.4236/NJGC.2013.32011
36. J. Wilson, G.H. Pigott, F.J. Schoen, L.L. Hench, Toxicology and biocompatibility of bioglasses. J. Biomed. Mater. Res. **15**(6), 805–817 (1981)
37. R.L. Gillette, S.F. Swaim, E.A. Sartin, D.M. Bradley, S.L. Coolman, Effects of a bioactive glass on healing of closed skin wounds in dogs. Am. J. Vet. Res. **62**(7), 1149–1153 (2001). https://doi.org/10.2460/AJVR.2001.62.1149
38. A.M.A. Coco, T. Martins, B.R. Barrioni, M.M. de Pereira, Effect of incorporating silver on the structure and ion release profile of binary SiO_2–Ag_2O mesoporous bioactive glass submicron

© The Author(s), under exclusive licence to The Materials Research Society 2023

spherical particles. Ceram. Int. **47**(18), 26100–26108 (2021). https://doi.org/10.1016/J.CERAMINT.2021.06.016

39. S. Kargozar, S. Hamzehlou, F. Baino, Can bioactive glasses be useful to accelerate the healing of epithelial tissues? Mater. Sci. Eng. C **97**, 1009–1020 (2019). https://doi.org/10.1016/J.MSEC.2019.01.028
40. G. Kaur, *Bioactive Glasses in Angiogenesis and Wound Healing : Soft Tissue Repair* (Springer, Cham, 2017), pp.237–260. https://doi.org/10.1007/978-3-319-45716-1_9
41. E. Mazzoni, M.R. Iaquinta, C. Lanzillotti, C. Mazziotta, M. Maritati, M. Montesi, S. Sprio, A. Tampieri, M. Tognon, F. Martini, Bioactive materials for soft tissue repair. Front. Bioeng. Biotechnol. (2021). https://doi.org/10.3389/FBIOE.2021.613787/BIBTEX
42. H. Li, J. He, H. Yu, C.R. Green, J. Chang, Bioglass promotes wound healing by affecting gap junction connexin 43 mediated endothelial cell behavior. Biomaterials **84**, 64–75 (2016). https://doi.org/10.1016/J.BIOMATERIALS.2016.01.033
43. W. Xie, X. Chen, G. Miao, J. Tang, X. Fu, Regulation of cellular behaviors of fibroblasts related to wound healing by sol–gel derived bioactive glass particles. J. Biomed. Mater. Res. A **104**(10), 2420–2429 (2016). https://doi.org/10.1002/JBM.A.35782
44. A.A. Gorustovich, J.A. Roether, A.R. Boccaccini, Effect of bioactive glasses on angiogenesis: a review of in vitro and in vivo evidences. Tissue Eng. Part B Rev. **16**(2), 199–207 (2010). https://doi.org/10.1089/ten.TEB.2009.0416
45. M. Jridi, S. Bardaa, D. Moalla, T. Rebaii, N. Souissi, Z. Sahnoun, M. Nasri, Microstructure, rheological and wound healing properties of collagen-based gel from cuttlefish skin. Int. J. Biol. Macromol. **77**, 369–374 (2015). https://doi.org/10.1016/J.IJBIOMAC.2015.03.020
46. J. Zhu, G. Jiang, G. Song, T. Liu, C. Cao, Y. Yang, Y. Zhang, W. Hong, Incorporation of ZnO/bioactive glass nanoparticles into alginate/chitosan composite hydrogels for wound closure. ACS Appl. Bio Mater. **2**(11), 5042–5052 (2019). https://doi.org/10.1021/ACSABM.9B00727/ASSET/IMAGES/LARGE/MT9B00727_0009.JPEG
47. M. Sohrabi, B.E. Yekta, H.R. Rezaie, M.R. Naimi-Jamal, C. Bijan, The influence of 3-glycidyloxypropyl trimethoxysilane on the rheological and in-vitro behavior of injectable composites containing 64S bioactive glass, chitosan, and gelatin. J. Appl. Polym. Sci. **138**, 50963 (2021). https://doi.org/10.1002/APP.50963
48. W. Xie, X. Fu, F. Tang, Y. Mo, J. Cheng, H. Wang, X. Chen, Dose-dependent modulation effects of bioactive glass particles on macrophages and diabetic wound healing. J. Mater. Chem. B **7**(6), 940–952 (2019). https://doi.org/10.1039/C8TB02938E
49. J. Shen, W. Gu, X. Yang, Y. Li, Z. Gou, Z. Jin, Systematic investigation of a new nanoscale bioactive glass on wound healing in vivo in comparison with the clinically applied 45S5 Bioglass. Int. J. Regener. Med. **2018**(1), 1–8 (2018). https://doi.org/10.31487/J.RGM.2018.10.001
50. S. Pourshahrestani, E. Zeimaran, N.A. Kadri, N. Gargiulo, S. Samuel, S.V. Naveen, T. Kamarul, M.R. Towler, Gallium-containing mesoporous bioactive glass with potent hemostatic activity and antibacterial efficacy. J. Mater. Chem. B **4**(1), 71–86 (2015). https://doi.org/10.1039/C5TB02062J
51. J. Li, D. Zhai, F. Lv, Q. Yu, H. Ma, J. Yin, Z. Yi, M. Liu, J. Chang, C. Wu, Preparation of copper-containing bioactive glass/egg-shell membrane nanocomposites for improving angiogenesis, antibacterial activity and wound healing. Acta Biomater. **36**, 254–266 (2016). https://doi.org/10.1016/J.ACTBIO.2016.03.011
52. C. Mao, C. Lin, X. Chen, Enhanced healing of full-thickness diabetic wounds using bioactive glass and Yunnan baiyao ointments. J. Wuhan Univ. Technol.-Mater. Sci. Ed. **29**(5), 1063–1070 (2014). https://doi.org/10.1007/S11595-014-1044-Y
53. S. Naseri, W.C. Lepry, S.N. Nazhat, Bioactive glasses in wound healing: hope or hype? J. Mater. Chem. B **5**(31), 6167–6174 (2017). https://doi.org/10.1039/C7TB01221G
54. L. Hupa, K.H. Karlsson, Tailoring of bioactive glasses, in *Bioactive Glasses: Fundamentals, Technology and Applications*, vol. 2017, ed. by A.R. Boccaccini, D.S. Brauer (Royal Society of Chemistry, London, 2016), pp.136–160
55. S. Majumdar, S. Gupta, S. Krishnamurthy, Multifarious applications of bioactive glasses in soft tissue engineering. Biomater. Sci. **9**(24), 8111–8147 (2021). https://doi.org/10.1039/D1BM01104A
56. I. Cacciotti, Bivalent cationic ions doped bioactive glasses: the influence of magnesium, zinc, strontium and copper on the physical and biological properties. J. Mater. Sci. **52**(15), 8812–8831 (2017). https://doi.org/10.1007/S10853-017-1010-0
57. K.H. Brown, S.E. Wuehler, J.M. Peerson, The importance of zinc in human nutrition and estimation of the global prevalence of zinc deficiency. Food Nutr. Bull. **22**(2), 113–125 (2016). https://doi.org/10.1177/156482650102200201
58. M.J. Jackson, Physiology of zinc: general aspects, in *Zinc in Human Body*. ed. by C.F. Mills (Springer, London, 1989), pp.1–14
59. Z. Neščáková, K. Zheng, L. Liverani, Q. Nawaz, D. Galusková, H. Kaňková, M. Michálek, D. Galusek, A.R. Boccaccini, Multifunctional zinc ion doped sol–gel derived mesoporous bioactive glass nanoparticles for biomedical applications. Bioact. Mater. **4**, 312–321 (2019). https://doi.org/10.1016/J.BIOACTMAT.2019.10.002
60. Y.F. Goh, A.Z. Alshemary, M. Akram, M.R. Abdul Kadir, R. Hussain, In vitro study of nano-sized zinc doped bioactive glass. Mater. Chem. Phys. **137**(3), 1031–1038 (2013). https://doi.org/10.1016/J.MATCHEMPHYS.2012.11.022
61. R. Sergi, D. Bellucci, R. Salvatori, G. Maisetta, G. Batoni, V. Cannillo, Zinc containing bioactive glasses with ultra-high crystallization temperature, good biological performance and

© The Author(s), under exclusive licence to The Materials Research Society 2023

antibacterial effects. Mater. Sci. Eng. C **104**, 109910 (2019). https://doi.org/10.1016/J.MSEC.2019.109910

62. V. Aina, G. Malavasi, A. Fiorio Pla, L. Munaron, C. Morterra, Zinc-containing bioactive glasses: surface reactivity and behaviour towards endothelial cells. Acta Biomater. **5**(4), 1211–1222 (2009). https://doi.org/10.1016/J.ACTBIO.2008.10.020
63. G. Lusvardi, G. Malavasi, L. Menabue, M.C. Menziani, A. Pedone, U. Segre, V. Aina, A. Perardi, C. Morterra, F. Boccafoschi et al., Properties of zinc releasing surfaces for clinical applications. J. Biomater. Appl. **22**(6), 505–526 (2007). https://doi.org/10.1177/0885328207079731
64. S. Solgi, M. Shahrezaee, A. Zamanian, T.S. Jafarzadeh Kashi, M. Raz, K. Khoshroo, M. Tahriri, Sol-gel synthesis and characterization of SiO_2-CaO-P_2O_5-SrO bioactive glass: In Vitro Study. Key Eng. Mater. **631**, 30–35 (2015). https://doi.org/10.4028/WWW.SCIENTIFIC.NET/KEM.631.30
65. Q. Nawaz, A. de Pablos-Martín, J.M. de Souza e Silva, L. Berthold, K. Hurle, A.T. Contreras Jaimes, M. Sitarz, D.S. Brauer, A.R. Boccaccini, Crystallization study of sol–gel derived 13–93 bioactive glass powder. J. Eur. Ceram. Soc. **41**(2), 1695–1706 (2021). https://doi.org/10.1016/J.JEURCERAMSOC.2020.09.052
66. A. Doostmohammadi, A. Monshi, R. Salehi, M.H. Fathi, Z. Golniya, A.U. Daniels, Bioactive glass nanoparticles with negative zeta potential. Ceram. Int. **37**(7), 2311–2316 (2011). https://doi.org/10.1016/J.CERAMINT.2011.03.026
67. D. Bellucci, V. Cannillo, A novel bioactive glass containing strontium and magnesium with ultra-high crystallization temperature. Mater. Lett. **213**, 67–70 (2018). https://doi.org/10.1016/J.MATLET.2017.11.020
68. N. Zhao, W. Yuan, Functionally integrated bioglass microspheres-composited double-network hydrogel with good tissue adhesion and electrical conductivity for efficient wound treatment and health detection. Compos. B Eng. **242**, 110095 (2022). https://doi.org/10.1016/J.COMPOSITESB.2022.110095
69. R. Chen, Q. Li, Q. Zhang, S. Xu, J. Han, P. Huang, Z. Yu, D. Jia, J. Liu, H. Jia et al., Nanosized HCA-coated borate bioactive glass with improved wound healing effects on rodent model. Chem. Eng. J. **426**, 130299 (2021). https://doi.org/10.1016/J.CEJ.2021.130299
70. A.M. El-Kady, A.F. Ali, Fabrication and characterization of ZnO modified bioactive glass nanoparticles. Ceram. Int. **38**(2), 1195–1204 (2012). https://doi.org/10.1016/J.CERAMINT.2011.07.069
71. S. Shruti, A.J. Salinas, G. Malavasi, G. Lusvardi, L. Menabue, C. Ferrara, P. Mustarelli, M. Vallet-Regì, Structural and in vitro study of cerium, gallium and zinc containing sol–gel bioactive glasses. J. Mater. Chem. **22**(27), 13698–13706 (2012). https://doi.org/10.1039/C2JM31767B
72. A. Haider, A. Waseem, N. Karpukhina, S. Mohsin, Strontium- and Zinc-containing bioactive glass and alginates scaffolds. Bioengineering **7**(1), 10 (2020). https://doi.org/10.3390/BIOENGINEERING7010010
73. A.C. Özarslan, S. Yücel, Evaluation of novel composition (SiO_2–CaO–Na_2O–P_2O_5, SrO–CuO) degradable amorphous silicate glasses properties and comprehensive characterization of the thermal features. Ceram. Int. (2022). https://doi.org/10.1016/J.CERAMINT.2022.10.228
74. N.S. Hussain, M.A. Lopes, J.D. Santos, A comparative study of CaO–P_2O5–SiO_2 gels prepared by a sol–gel method. Mater. Chem. Phys. **88**(1), 5–8 (2004). https://doi.org/10.1016/J.MATCHEMPHYS.2004.06.015
75. M. Blochberger, L. Hupa, D.S. Brauer, Influence of zinc and magnesium substitution on ion release from Bioglass 45S5 at physiological and acidic pH. Biomed. Glasses **1**(1), 93–107 (2015). https://doi.org/10.1515/BGLASS-2015-0009/MACHINEREADABLECITATION/RIS
76. S.M. Rabiee, N. Nazparvar, M. Azizian, D. Vashaee, L. Tayebi, Effect of ion substitution on properties of bioactive glasses: a review. Ceram. Int. **41**(6), 7241–7251 (2015). https://doi.org/10.1016/J.CERAMINT.2015.02.140
77. A.J. Salinas, S. Shruti, G. Malavasi, L. Menabue, M. Vallet-Regí, Substitutions of cerium, gallium and zinc in ordered mesoporous bioactive glasses. Acta Biomater. **7**(9), 3452–3458 (2011). https://doi.org/10.1016/J.ACTBIO.2011.05.033
78. S. Shahrabi, S. Hesaraki, S. Moemeni, M. Khorami, Structural discrepancies and in vitro nanoapatite formation ability of sol–gel derived glasses doped with different bone stimulator ions. Ceram. Int. **37**(7), 2737–2746 (2011). https://doi.org/10.1016/J.CERAMINT.2011.04.025
79. C. B. Çevlik, Sodyum hiyalüronat ve stronsiyum-çinko katkılı biyoaktif cam içerikli doku iskelesi üretimi ve karakterizasyonu / Production and characterization of tissue scaffold contain sodium hyaluronate and strontium-zinc doped 45S5 bioactive glass. Yıldız Technical University, (2020).
80. T.A. Ostomel, Q. Shi, C.K. Tsung, H. Liang, G.D. Stucky, Spherical bioactive glass with enhanced rates of hydroxyapatite deposition and hemostatic activity. Small **2**(11), 1261–1265 (2006). https://doi.org/10.1002/SMLL.200600177
81. U. Wollina, K. Hasenöhrl, E. Köstler, J. Schönlebe, B. Heinig, G. Haroske, T. Kittner, Dystrophic calcification in chronic leg ulcers—a clinicopathologic study. Dermatol. Surg. **35**(3), 457–461 (2009). https://doi.org/10.1111/J.1524-4725.2009.01064.X
82. S. Tokoro, T. Satoh, Y. Okubo, K. Igawa, H. Yokozeki, Latent dystrophic subcutaneous calcification in patients with chronic venous insufficiency. Acta Derm. Venereol. **89**(5), 505–508 (2009). https://doi.org/10.2340/00015555-0680/
83. E. Norris, *Bioactive Glass Scaffolds for Wound Healing* (Imperial College London, London, 2019)
84. P.C.M. Van De Kerkhof, J. Berth-Jones, C.E.M. Griffiths, P.V. Harrison, H. Hönigsmann, R. Marks, R. Roelandts, E. Schöpf,

© The Author(s), under exclusive licence to The Materials Research Society 2023

C. Trompke, Long-term efficacy and safety of tacalcitol ointment in patients with chronic plaque psoriasis. Br. J. Dermatol. **146**(3), 414–422 (2002). https://doi.org/10.1046/J.1365-2133.2002.04567.X

85. E.K. Park, K.W. Song, Rheological evaluation of petroleum jelly as a base material in ointment and cream formulations: steady shear flow behavior. Arch. Pharm. Res. **33**(1), 141–150 (2010). https://doi.org/10.1007/S12272-010-2236-4
86. P. M. Doran, Fluid flow, in *Bioprocess Engineering Principles* (2013), pp. 201–254. https://doi.org/10.1016/B978-0-12-220851-5.00007-1.
87. H.P. Rønningsen, Rheology of petroleum fluids. Annu. Trans. Nordic Rheol. Soc. **20**, 11–18 (2012)
88. Y.S. Wu, Immiscible displacement of non-Newtonian fluids, in *Multiphase Fluid Flow in Porous and Fractured Reservoirs*. ed. by Y.S. Wu (Elsevier, Amsterdam, 2016), pp.127–166
89. J.P. Marty, C. Lafforgue, J.L. Grossiord, P. Soto, Rheological properties of three different vitamin D ointments and their clinical perception by patients with mild to moderate psoriasis. J. Eur. Acad. Dermatol. Venereol. **19**(3), 7–10 (2005). https://doi.org/10.1111/J.1468-3083.2005.01330.X
90. A.C. Özarslan, Y.B. Elalmis, S. Yücel, Production of biosilica based bioactive glass-alginate composite putty as bone support material, and evaluation of in vitro properties; bioactivity and cytotoxicity behavior. J. Non Cryst. Solids **561**, 120755 (2021). https://doi.org/10.1016/J.JNONCRYSOL.2021.120755
91. B.E. Rapp, Fluids, in *Microfluidics: Modelling, Mechanics and Mathematics*. ed. by B. Rapp (Elsevier, Amsterdam, 2017), pp.243–263. https://doi.org/10.1016/B978-1-4557-3141-1.50009-5
92. R.P. Chhabra, Non-Newtonian fluids: an introduction. Rheol. Complex Fluids (2010). https://doi.org/10.1007/978-1-4419-6494-6_1/FIGURES/23
93. F. Walha, K. Lamnawar, A. Maazouz, M. Jaziri, Rheological, morphological and mechanical studies of sustainably sourced polymer blends based on poly(lactic acid) and polyamide 11. Polymers **8**(3), 61 (2016). https://doi.org/10.3390/POLYM8030061
94. R. Ganguly, S. Kumar, A. Kunwar, S. Nath, H.D. Sarma, A. Tripathi, G. Verma, D.P. Chaudhari, V.K. Aswal, J.S. Melo, Structural and therapeutic properties of curcumin solubilized pluronic F127 micellar solutions and hydrogels. J. Mol. Liq. **314**, 113591 (2020). https://doi.org/10.1016/J.MOLLIQ.2020.113591
95. R. Ganguly, G. Verma, A. Ingle, S. Kumar, H.D. Sarma, D. Dutta, B. Dutta, A. Kunwar, K. Ajish, K.C. Bhainsa et al., Structural, rheological and therapeutic properties of pluronic F127 hydrogel and beeswax based lavender oil ointment formulations. J. Mol. Liq. **365**, 120157 (2022). https://doi.org/10.1016/J.MOLLIQ.2022.120157
96. M.S. Kwak, H.J. Ahn, K.W. Song, Rheological investigation of body cream and body lotion in actual application conditions. Korea-Aust. Rheol. J. **27**(3), 241–251 (2015). https://doi.org/10.1007/S13367-015-0024-X
97. S. Patere, B. Newman, Y. Wang, S. Choi, S. Vora, A.W.K. Ma, M. Jay, X. Lu, Influence of manufacturing process variables on the properties of ophthalmic ointments of tobramycin. Pharm. Res. **35**(9), 1–16 (2018). https://doi.org/10.1007/S11095-018-2462-X/FIGURES/10
98. P. Pandey, G.D. Ewing, Rheological characterization of petrolatum using a controlled stress rheometer. Drug Dev. Ind. Pharm. **34**(2), 157–163 (2009). https://doi.org/10.1080/03639040701484569
99. A. Lauterbach, K. Ekelund, Rheological temperature sweeping in a quality by design approach for formulation development and optimization. Int. J. Pharm. **568**, 118533 (2019). https://doi.org/10.1016/J.IJPHARM.2019.118533
100. J. Nanda, A. Banerjee, β-Amino acid containing proteolitically stable dipeptide based hydrogels: encapsulation and sustained release of some important biomolecules at physiological pH and temperature. Soft Matter **8**(12), 3380–3386 (2012). https://doi.org/10.1039/C2SM07168A/
101. C. Pontremoli, M. Boffito, S. Fiorilli, R. Laurano, A. Torchio, A. Bari, C. Tonda-Turo, G. Ciardelli, C. Vitale-Brovarone, Hybrid injectable platforms for the in situ delivery of therapeutic ions from mesoporous glasses. Chem. Eng. J. **340**, 103–113 (2018). https://doi.org/10.1016/J.CEJ.2018.01.073
102. Á.J. Leite, B. Sarker, T. Zehnder, R. Silva, J.F. Mano, A.R. Boccaccini, Bioplotting of a bioactive alginate dialdehyde-gelatin composite hydrogel containing bioactive glass nanoparticles. Biofabrication (2016). https://doi.org/10.1088/1758-5090/8/3/035005
103. M. Ojansivu, A. Rashad, A. Ahlinder, J. Massera, A. Mishra, K. Syverud, A. Finne-Wistrand, S. Miettinen, K. Mustafa, Wood-based nanocellulose and bioactive glass modified gelatin-alginate bioinks for 3D bioprinting of bone cells. Biofabrication (2019). https://doi.org/10.1088/1758-5090/AB0692
104. J. Huang, C. Zhong, X. Wu, Shear behavior at high pressures and viscoelastic properties in water and in brine solutions with high salinities for a tetra-polymer containing poly(ethylene oxide) side chains. RSC Adv. **7**(75), 47624–47635 (2017). https://doi.org/10.1039/C7RA09771A
105. M.C. Milliatti, S.C. da SilvaLannes, Impact of stabilizers on the rheological properties of ice creams. Food Sci. Technol. **38**(4), 733–739 (2018). https://doi.org/10.1590/FST.31818
106. M. Andjić, N. Draginić, A. Kočović, J. Jeremić, K. Vučićević, N. Jeremić, V. Krstonošić, B. Božin, N. Kladar, I. Čapo et al., Immortelle essential oil-based ointment improves wound healing in a diabetic rat model. Biomed. Pharmacother. **150**, 112941 (2022). https://doi.org/10.1016/J.BIOPHA.2022.112941
107. H. Fathalipour-Rayeni, H. Forootanfar, P. Khazaeli, M. Mehrabani, H.R. Rahimi, M. Shakibaie, E. Jafari, M. Doostmohammadi, M.S. Bami, M. Adeli-Sardou et al., Evaluation of antioxidant

© The Author(s), under exclusive licence to The Materials Research Society 2023

potential of Heliotropium bacciferum Forssk extract and wound healing activity of its topical formulation in rat. Ann. Pharm. Fr. **80**(3), 280–290 (2022). https://doi.org/10.1016/J.PHARMA.2021.09.005

108. D. Risica, A. Barbetta, L. Vischetti, C. Cametti, M. Dentini, Rheological properties of guar and its methyl, hydroxypropyl and hydroxypropyl-methyl derivatives in semidilute and concentrated aqueous solutions. Polymer (Guildf) **51**(9), 1972–1982 (2010). https://doi.org/10.1016/J.POLYMER.2010.02.041
109. T. Ivko, V. Hrytsenko, L. Kienko, L. Bobrytska, H. Kukhtenko, T. Germanyuk, Investigation of the rheological properties of ointment bases as a justification of the ointment composition for herpes treatment. Turk. J. Pharm. Sci. **18**(5), 628 (2021). https://doi.org/10.4274/TJPS.GALENOS.2021.93457
110. A. Wajda, W.H. Goldmann, R. Detsch, A.R. Boccaccini, M. Sitarz, Influence of zinc ions on structure, bioactivity, biocompatibility and antibacterial potential of melt-derived and gel-derived glasses from CaO-SiO_2 system. J. Non Cryst. Solids **511**, 86–99 (2019). https://doi.org/10.1016/J.JNONCRYSOL.2018.12.040
111. F. Chai, A.Q. Truong-Tran, L.H. Ho, P.D. Zalewski, Regulation of caspase activation and apoptosis by cellular zinc fluxes and zinc deprivation: a review. Immunol. Cell Biol. **77**(3), 272–278 (1999). https://doi.org/10.1046/J.1440-1711.1999.00825.X
112. D.W. Choi, J.Y. Koh, Zionc and brain injury. Annu. Rev. Neurosci. **21**, 347 (1998)
113. S. Kapoor, A. Goel, A.F. Correia, M.J. Pascual, H.Y. Lee, H.W. Kim, J.M.F. Ferreira, Influence of ZnO/MgO substitution on sintering, crystallisation, and bio-activity of alkali-free glass-ceramics. Mater. Sci. Eng. C **53**, 252–261 (2015). https://doi.org/10.1016/J.MSEC.2015.04.023
114. G. Erel-Akbaba, H. Akbaba, E. Keselik, S.A. Bahceci, Z. Senyigit, T.K. Temiz, Octaarginine functionalized nanoencapsulated system: In vitro and in vivo evaluation of bFGF loaded formulation for wound healing. J. Drug Deliv. Sci. Technol. **71**, 103343 (2022). https://doi.org/10.1016/J.JDDST.2022.103343
115. S. Gunes, S. Tamburaci, M.C. Dalay, I.D. Gurhan, In vitro evaluation of Spirulina platensis extract incorporated skin cream with its wound healing and antioxidant activities. Pharm. Biol. **55**(1), 1824–1832 (2017). https://doi.org/10.1080/13880209.2017.1331249
116. C. Mao, X. Chen, G. Miao, C. Lin, Angiogenesis stimulated by novel nanoscale bioactive glasses. Biomed. Mater. **10**(2), 025005 (2015). https://doi.org/10.1088/1748-6041/10/2/025005
117. A.C. Özarslan, S. Yücel, Fabrication and characterization of strontium incorporated 3-D bioactive glass scaffolds for bone tissue from biosilica. Mater. Sci. Eng. C **68**, 350–357 (2016). https://doi.org/10.1016/J.MSEC.2016.06.004
118. R. Hill, An alternative view of the degradation of bioglass. J. Mater. Sci. Lett. **15**(13), 1122–1125 (1996). https://doi.org/10.1007/BF00539955
119. M.D. O'Donnell, R.G. Hill, Influence of strontium and the importance of glass chemistry and structure when designing bioactive glasses for bone regeneration. Acta Biomater. **6**(7), 2382–2385 (2010). https://doi.org/10.1016/J.ACTBIO.2010.01.006
120. I. Farooq, Z. Imran, U. Farooq, A. Leghari, H. Ali, S. Patil, Bioactive glass: a material for the future. World J. Dent. **3**(2), 199–201 (2012). https://doi.org/10.5005/JP-JOURNALS-10015-1156
121. S. Borhan, S. Hesaraki, A.A. Behnamghader, E. Ghasemi, Rheological evaluations and in vitro studies of injectable bioactive glass–polycaprolactone–sodium alginate composites. J. Mater. Sci. Mater. Med. **27**(9), 1–15 (2016). https://doi.org/10.1007/S10856-016-5745-Y/FIGURES/12
122. ISO, 10993–5, *2009: Biological Evaluation of Medical Devices—Part 5: Tests for In Vitro Cytotoxicity* (Switzerland, Geneva, 2009)
123. P.S. de Gomes, M.H. Figueiral, M.H.R. Fernandes, C. Scully, Cytotoxicity of denture adhesives. Clin. Oral Investig. **15**(6), 885–893 (2011). https://doi.org/10.1007/S00784-010-0464-0/FIGURES/3
124. M. Allaw, M. Manconi, P. Caboni, G. Bacchetta, E. Escribano-Ferrer, J.E. Peris, A. Nacher, O. Diez-Sales, M.L. Manca, Formulation of liposomes loading lentisk oil to ameliorate topical delivery, attenuate oxidative stress damage and improve cell migration in scratch assay. Biomed. Pharmacother. (2021). https://doi.org/10.1016/J.BIOPHA.2021.112351

Publisher's Note Springer Nature remains neutral with regard to jurisdictional claims in published maps and institutional affiliations.

Springer Nature or its licensor (e.g. a society or other partner) holds exclusive rights to this article under a publishing agreement with the author(s) or other rightsholder(s); author self-archiving of the accepted manuscript version of this article is solely governed by the terms of such publishing agreement and applicable law.

© The Author(s), under exclusive licence to The Materials Research Society 2023